Sheffield Hallam University

Hardness of porous nanocrystalline Co-Ni electrodeposits

MA, C., WANG, S.C., WOOD, R.J.K., ZEKONYTE, J., LUO, Quanshun <http://orcid.org/0000-0003-4102-2129> and WALSH, F.C.

Available from Sheffield Hallam University Research Archive (SHURA) at:

http://shura.shu.ac.uk/26057/

This document is the author deposited version. You are advised to consult the publisher's version if you wish to cite from it.

Published version

MA, C., WANG, S.C., WOOD, R.J.K., ZEKONYTE, J., LUO, Quanshun and WALSH, F.C. (2013). Hardness of porous nanocrystalline Co-Ni electrodeposits. Metals and Materials International, 19 (6), 1187-1192.

Copyright and re-use policy

See http://shura.shu.ac.uk/information.html

Sheffield Hallam University Research Archive
http://shura.shu.ac.uk

The hardness of porous nano-crystalline Co-Ni electrodeposits

C. Ma[1], S.C. Wang[1], R. J. K. Wood[1], J. Zekonyte[1], Q. Luo[2], F. C. Walsh[3]

[1]University of Southampton, National Centre for Advanced Tribology at Southampton (nCATS), SO17 1BJ, UK
[2]2Sheffield Hallam University, Materials and Engineering Research Institute, Sheffield, S1 1WB, UK
[3]University of Southampton, Engineering Materials and Surface Engineering, Engineering and the Environment, SO17 1BJ, UK

Keywords: hardness, nanocrystalline, hall-petch relationship, porosity, Co-Ni

Abstract

The Hall-Petch relationship can fail when the grain size is below a critical value of tens of nanometres. This occurs particularly for coatings having porous surfaces. In this study, electrodeposited nanostructured Co-Ni coatings from four different nickel electroplating baths having grain sizes in the range of 11-23 nm have been investigated. The finest grain size, approximately 11 nm, was obtained from a coating developed from the nickel sulphate bath. The Co-Ni coatings have a mixed face centred cubic and hexagonal close-packed structures with varying surface morphologies and different porosities. A cluster-pore mixture model has been proposed by considering no contribution from pores to the hardness. As the porosity effect was taken into consideration, the calculated pore-free hardness is in agreement with the ordinary Hall-Petch relationship even when the grain size is reduced to 11 nm for the Co-Ni coatings with 77±2 at% cobalt. The present model was applied to other porous nanocrystalline coatings, and the Hall-Petch relationship was maintained.

1 Introduction

Nanocrystalline Co-Ni coatings have the potential to be used in aerospace, automobile and general engineering industries due to their high strength, good wear-resistance and high anti-corrosion resistance [1]. These coatings are commonly deposited from plating baths which contain one or two types of nickel salts - sulphate and chloride for different applications. For example, coatings deposited from a nickel chloride bath can be used in the decorative industry for anticorrosion applications but not in engineering applications as a high internal stress limits the coating thickness (less than 2.5 μm). Although the effect of baths with different nickel salts on mechanical properties has been studied on coarse-grained (grain size of the order of microns) nickel coatings with a low hardness, typically below 300 HV [2], there are few comparable studies for nanocrystalline Co-Ni coatings.

Polycrystalline metals show an increase of yield stress with the decrease of grain size. This is known as the Hall- Petch effect [3]. It can be applied to Vickers hardness which is approximately three times the compressive yield stress if a small amount work-hardening occurs. Nanocrystalline materials (grain size below 100 nm) can show enhanced physical, mechanical and chemical properties compared with their coarse-grained counterparts [4]. However, with a further refined grain size of nanocrystals, it has been reported that the Hall- Petch slope becomes

smaller or even negative when the grain size is reduced to a threshold value [5]. Previous studies indicated that a deviation from the conventional Hall-Petch relationship occurs when the grain size is below 50 - 60 nm for both electrodeposited Ni and Co [6,7]. Many mechanisms have been proposed, including increasing porosity of deposits with small grain size [8], larger fraction of atoms at grain boundaries [5], suppression of dislocation pile-ups [9] and the thermally-activated grain boundary shearing model [10]. Although electrodeposition was claimed to produce porosity-free products [11], the present authors noticed that the as-deposited nickel and cobalt coatings [6,7] consist of a mixture of clusters and pores, in which a cluster contains tens and hundreds of nanocrystalline grains. Deviation from the Hall-Petch relationship may derive from the porosity, which needs to be clarified. Hence, in the present study, nanocrystalline Co-Ni coatings with different porosities were investigated. The porosity was varied by controlling the concentration of nickel sulphate and nickel chloride within the electroplating bath.

Table 1. The bath compositions employed for Co-Ni electrodeposition

Bath component	Bath composition / g dm^{-3}			
	A1	A2	A3	A4
$NiSO_4 \cdot 6H_2O$	200	200	0	50
$NiCl_2 \cdot 6H_2O$	0	50	200	200
$CoSO_4 \cdot 7H_2O$	100	100	100	100
Boric acid	30	30	30	30
Saccharin	2	2	2	2

2 Experimental procedures

As shown in Table 1, four coatings were deposited from electrolytes containing different concentrations of various nickel salts (A1 - A4). The bath temperature was maintained at 45 °C. The samples were electrodeposited using a constant current density of 4 A dm−2. The solution is continuously stirred by a PTFE-coated magnetic stirrer bar (6 mm diameter × 30 mm length) at 200 rpm. The anode was a high purity Ni sheet (40 mm × 10 mm × 1 mm) while the substrate was mild steel AISI 1020 (40 mm × 10 mm × 2 mm) as the cathode. The electrodes were held parallel to each other with an interelectrode gap of 25 mm. All the thicknesses of the coatings were 50 ± 2 μm. The surface of the as-deposited Co-Ni coating was investigated by a JEOL JSM-6500 scanning electron microscope (SEM) while the composition of the alloys was determined by electron dispersive spectrometry (EDS). The surface roughness of the as-deposited Co-Ni coating was measured by an Agilent 5500 atomic force microscope (AFM). A line profile (5 μm) with height measurements was used to determine the surface roughness. Five measurements were performed on each coating. The crystal structure, as well as the grain size, was studied by a Bruker GADDS Xray diffractometer (XRD) using CuKα radiation. The residual stress was measured by a computer programmed Philips X-Pert X-ray diffractometer using CuKα radiation source by the sin2 ψ technique. A JEOL JEM-3010 transmission electron microscope (TEM) at 300 kV was employed to measure the grain size, while the phase structure was examined by selected area electron diffraction (SAED). The hardness of deposits was measured by a Vickers hardness indenter under an applied load of 100 g for a dwell time of 15 s. 5 measurements were carried out on each coating.

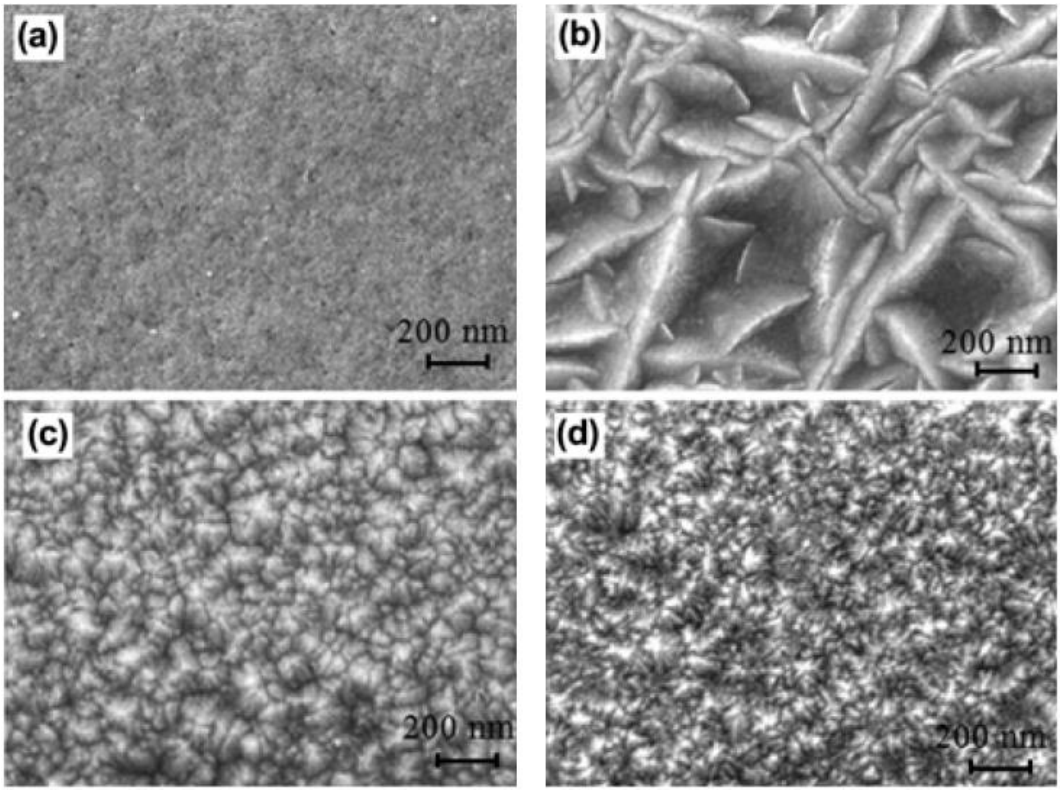

Fig. 1. SEM images of as-deposited Co-Ni alloys (a) A1 from the allsulphate bath with a dense and smooth surface, (b) A2 from the sulphate-dominant bath giving rise to a lens-shaped microstructure consisting of smaller grains, (c) A3 from the chloride-dominant bath and (d) A4 from the all-chloride bath showing clusters in the deposits.

3 Results and discussion

3.1. Surface morphologies and composition

Figure 1 shows high resolution SEM surface morphologies of four Co-Ni coatings (A1 - A4) deposited from different electroplating baths. Coating A1 deposited from an all sulphate bath has a dense and smooth surface (Fig. 1a) with low value of roughness (Ra = 10 nm). The grain was too fine to be resolved by SEM. With the addition of nickel chloride in the bath, the microstructure of coating A2 has dramatically changed to lens shape (Fig. 1b) and the surface roughness increased to approximately 120 nm. A lens actually consists of a number of fine grains. Both A3 and A4 coatings were deposited from baths with high concentrations of Cl^-, and microcracks were observed by optical microscopy. Their surfaces have clusters consisting of fine grains as shown in Figs. 1(c, d) with the surface roughness of 35 nm and 22 nm, respectively. The EDS results confirm that four coatings (A1-A4) have the similar Co contents of 77 ± 2 at%, which reveals that the use of baths containing different types and levels of nickel salts has no significant effect on the composition of the Co-Ni coatings.

3.2. Microstructure and internal stress

The phase structure and grain size were further investigated by means of XRD and TEM. The XRD patterns for all samples (Fig. 2) exhibit a single peak. This indicates that all the coatings

have a strong texture, i.e. one particular plane is parallel to the coating surface. The peak at 0.205 nm

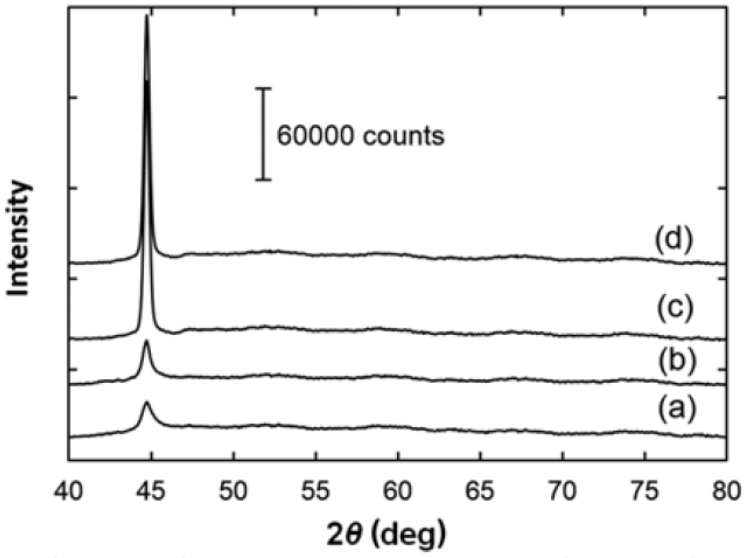

Fig. 2. XRD patterns of as-deposited Co-Ni alloys: A1 (a) and A2 (b) coatings deposited from the baths with lower concentration of nickel chloride than the baths of the sample A3 (c) and A4 (d).

(2θ = 44.5°) is consistent with the spacing of (111) in a face centred cubic (fcc) structured Co and/or (0002) hexagonal close-packed (hcp) structured Co lattice. The TEM electron diffraction patterns of the coatings are similar as shown in Figs. 3(b, d, f). A mixed structure of fcc (α) and hcp (ε) has been indexed in Fig. 3(d). The A1 coating deposited from the all-sulphate bath and the A2 deposited from the sulphate dominant baths have much lower peak intensities than A3 and A4. The XRD peak broadening is attributed to the small grain size, which was calculated by applying the Scherrer equation [12]:

$$d = \frac{0.9\lambda}{B\cos\theta} \qquad (1)$$

where λ is the wavelength of the X-rays (0.154 nm for Cu Kα radiation) and θ is the Bragg diffraction angle. B is the full width at half maximum height (FWHM) of the peak (in radians). The result of the grain sizes is listed in Table 2. TEM dark field images (Figs. 3(a, c, e)) were also taken to confirm the grain sizes. The measurements were carried out on at least 50 grains. The A3 coating from the all-chloride bath could not be successfully prepared for TEM foil because of its high brittleness.

The comparison of grain sizes in Table 2 shows the values calculated by Scherrer equation are consistent with those measured by TEM. It was reported that the total XRD peak broadening is attributed to both microstrain and the grain size [13]. In the present research, the peak broadening introduced by the microstrain is negligible. It has been widely accepted that nickel coatings deposited from baths containing high concentration of nickel chloride (samples A3 and A4) tend to have a higher internal stress than that from sulphate baths (the sample A1) or sulphamate baths [2]. The internal stress of samples A1 and A3 was measured by the XRD-sin2 ψ analysis method. The d-spacing dφψ of the (hkl) lattice plane can be described as [14]:

$$d_{\phi\psi} = \left(\frac{1+\nu}{E}\right)\sigma d_0 \sin^2\psi + \left(1-\frac{2\nu}{E}\sigma\right)d_0 \qquad (2)$$

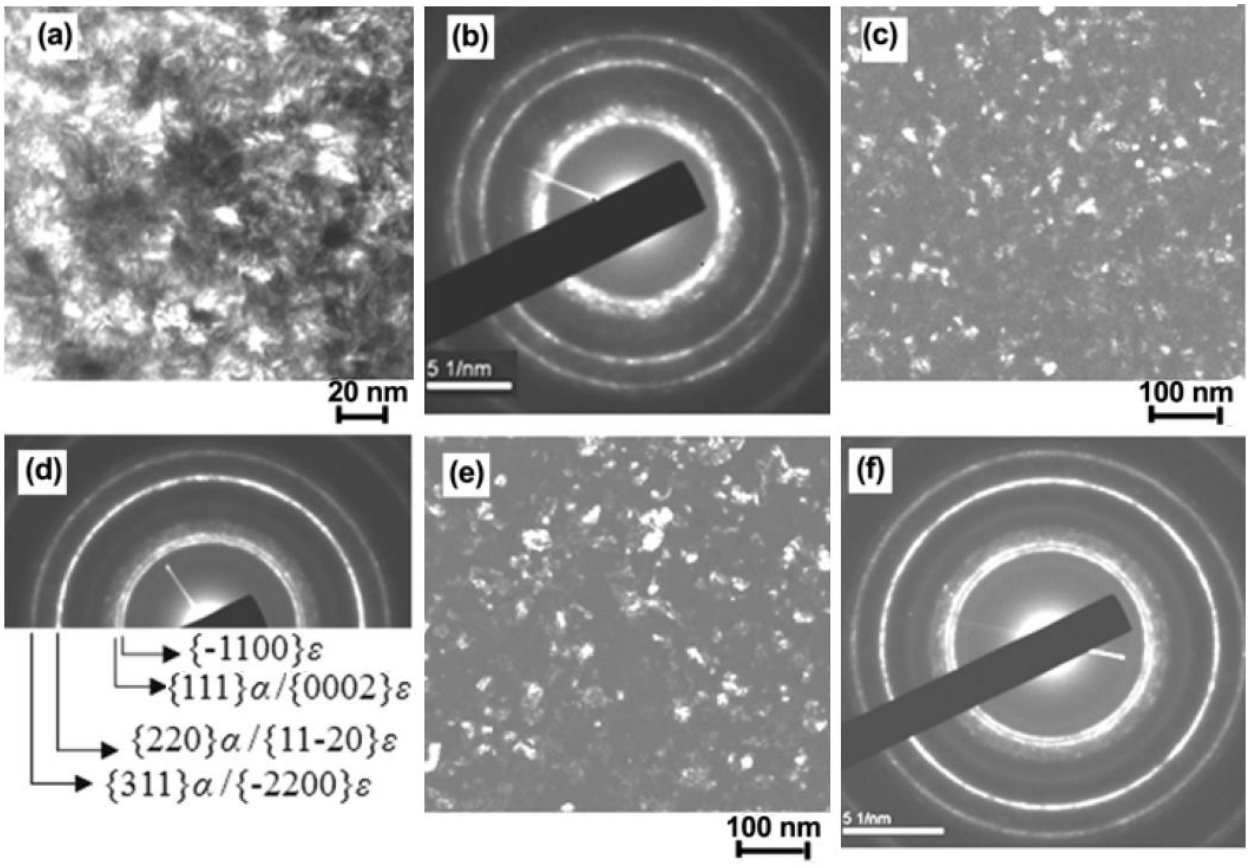

Fig. 3. Dark field images, and corresponding SAED patterns of the asdeposited Co-Ni alloys: A1 from all-sulphate bath (a, b), A2 from the sulphate dominant bath (c, d), A4 from the chloride dominant bath (e, f). SAED patterns indicated that the coatings have similar mixed structure of fcc (α) and hcp (ε).

Table 2. Comparison of grain sizes and hardness of the Co-Ni coatings

	Deposit			
	A1	A2	A3	A4
Grain size, *d* obtained by XRD / nm	11.3	14.5	22.7	22.6
Grain size obtained by TEM / nm	10±2	15±1	*	21±2
Measured hardnes, H_m / HV	503±5	379±20	455±7	469±8
Cluster size, d_{cl} / nm	11	162	30	24
Approximate surface poroxity, *p*	0	0.225	0.029	0.005
Calculated pore-free hardness, H_c by Eq. 7 / HV	503	489	468	471

*The TEM foil could not be prepared due to its high brittleness.

where E and v are the Young's modulus and the Poisson's ratio, respectively. σ is the internal stress, d0 is the lattice spacing at stress-free condition, and ψ is the off-axis angle with respect to the sample surface normal. The internal stress is related to the slope and the intercept of the plot of dφψ versus sin2 ψ. In the present research, the d-spacing measurements were conducted on the (111) plane at ψ ranging from -17° to 17°. The A3 coating has lower internal stress of 0.32

GPa than the A1 sample (1.05 GPa). This might be due to microcracks or free boundary clusters which can release the high internal stress.

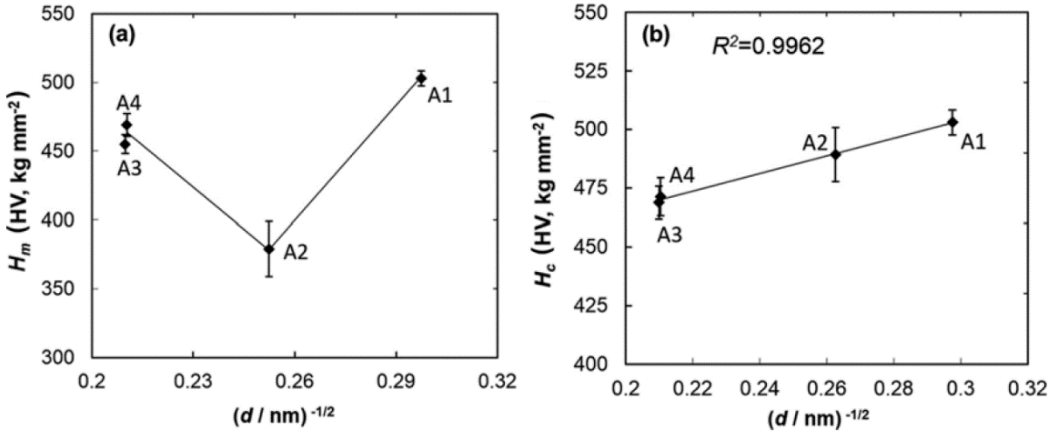

Fig. 4. Hall-Petch plots for as-deposited Co-Ni alloys before (a) and after (b) adopting the calculated pore-free hardness.

3.3. Microhardness

The measured hardness (Hm) of nanocrystalline Co-Ni alloys deposited from the baths containing different nickel salts is listed in the third row of Table 2. The Hall-Petch relationship [3] can be described as:

$$H = H_0 + kd^{-\frac{1}{2}} \quad (3)$$

where H0 is the intrinsic hardness, d is the grain size and k is a constant for a particular material. The measured hardness variation with the grain size (d) of the samples is plotted in the form of a Hall-Petch relationship in Fig. 4(a). The hardness against the reciprocal square root of grain size is not in agreement with the Hall-Petch relationship. In comparison with the sample A1, the coatings A3 and A4 have slightly lower hardness as a result of the increased grain size (23 nm) as shown in Fig. 4(a). There is, however, an anomalously low hardness (379 HV) for the sample A2 with the fine grain size of 15 nm. It might suggest that the anomaly of the coating A2 is caused by a loose microstructure containing the high porosity shown in Fig. 1(b). Its relatively high standard deviation of hardness measurements shown in Fig. 4(a) is due to the porosity. The comparison between the SEM image (Fig. 1b) and the TEM image (Fig. 3c) reveals that a lens is not a single grain but a cluster of hundreds of fine grains (around 15 nm). The lens-shaped cluster can be approximated as an ellipsoid with the same axis with lens shape. The size of the cluster (dcl) is estimated by calculating the equivalent spherical diameter, which is the diameter of a sphere having the same volume as the cluster [15]. The equation can be described as:

$$d_{cl} = 2\sqrt[3]{abc} \quad (4)$$

where a and b are the equatorial radii which are equal to each other and c is the polar radius. The mathematical expectation of the cluster size is calculated as 162 nm. The clusters of the sample A3 and A4 shown in Figs. 1(c, d) are simplified as spheroids, and the cluster sizes of which are 30 nm and 24 nm, respectively. According to the SEM images (Fig. 1), the porosity (p) of the present samples is described as the ratio of the volume of voids to the total volume of the surface layer [16], which can be estimated by:

$$p = \frac{V_t - N \times \frac{4}{3}\pi (d_d/2)^3}{V_t} \quad (5)$$

where Vt is the total deposit volume of the top surface and N is the measured number of clusters. The sample A1 is assumed to be free of pores (p = 0) due to its dense microstructure shown in the high-resolution SEM image (Fig. 1a). The results are listed in Table 2. According to the phase mixture model [4,17,18], for a nanostructured the crystallites, grain boundaries, triple line junctions and quadratic nodes have different contribution to the hardness and the yield strength depending on the individual volume fraction. However, the effect of cluster porosity has not been taken in account. The coatings in the present research can be considered as a mixture of clusters and pores with varied volume fractions, which can be expressed in terms of the porosity. The measured hardness is described as:

$$H_m = H_c(1-p) + H_p p \quad (6)$$

where Hc and Hp are the hardness contribution of clusters and pores, respectively. Hc is actually referring to H given by Eq. 3, which represents the hardness of the dense pore free coatings. In this cluster-pore mixture model, because pores have no contribution to the hardness (Hp≡0), the hardness of the cluster consisting of fine grains can be determined as:

$$H_c = \frac{H_m}{1-p} \quad (7)$$

The calculated pore-free hardness according to Eq. 7 is listed in Table 2. After adopting Hc as the hardness for Hall-Petch relationship, it can be observed that the hardness increases with a nearly constant slope and there is no obvious deviation even when the grain size is reduced to 11 nm as shown in Fig. 4(b). It is worth mentioning that in the Vickers hardness tests no cracking of coatings occurred with an applied load of 100 g. Therefore, these microcracks are not considered as surface pores. The hardness measurements have been found to be sensitive to microstructural flaws in the samples, particularly the porosity. In high-quality copper samples produced by inert gas condensation and compaction, the hardness is in agreement with the ordinary Hall-Petch relationship when the grain size is reduced to 15 nm, and then plateaued [19]. Sanders et al. [19] explained the deviation of the Hall-Petch relationship by increasing porosity of the samples with smaller grain size, which were produced by lower temperature compaction. Ibañez and Fatás [20] reported the Hall-Petch relationship in electrodeposited Cu coatings broke down when the grain size was less than 80 nm as shown in Fig. 5. From SEM images in the paper [20], the surface of the Cu coatings plated at different current densities consisted of clusters of different sizes. The porosity is calculated and the Hall-Petch plot with the pore-free hardness obtained by Eq. 7 has been redrawn. As shown in Fig. 5, the data fit the relationship well and a correlation coefficient (R2 = 0.9911) was obtained. Therefore, for the pore-free surface, the relationship between hardness and grain size may satisfy the Hall-Petch equation. However, for coatings with porous surfaces, the porosity effect needs to be taken into consideration for the validation of Hall-Petch equation. The calculated pore-free hardness rather than the measure hardness should be adopted.

4. CONCLUSIONS

The Co-Ni coatings (77 ± 2 at% Co) have been successfully prepared by electrodeposited from the bath with different nickel salts (nickel sulphate and / or nickel chloride), which were found to

have significant effects on the morphologies, grain sizes and hardness of the coatings. The following conclusions were drawn:

(1) The coating deposited from an all-sulphate bath is characterised by its dense and smooth surface with the finest grain size (approximately 11 nm). By adding nickel chloride in the bath, the coating has the porous lens-shaped microstructure

consisting of a number of fine grains (around 15 nm). The surfaces of the coatings plated from the chloride dominant bath and the all-chloride bath have clusters with much smaller size than that of the lens-shaped clusters. The grain size increased to approximately 23 nm.

(2) The hardness of porous coatings except the dense coating deposited from an all-sulphate bath exhibits the deviation of the Hall-Petch relationship. The extent of deviation depends on the porosity of coatings.

(3) By considering porous materials as composites of clusters and pores, their contribution to hardness has been quantitatively studied. The pore-free hardness (i.e. the hardness of clusters) can be calculated according to the cluster-pore mixture model. By adopting it, the Hall-Petch relationship can be maintained at nanoscale.

5. REFERENCES

1. L. Wang, Y. Gao, Q. Xue, H. Liu, and T. Xu, Appl. Surf. Sci. 242, 326 (2005).
2. M. Schlesinger, Modern Electroplating, 5th ed., p.91, John Wiley & Sons, Inc., New Jersey (2011).
3. A. Kelly and R. B. Nicholson, Strengthening Methods in Crystals, p.333, Elsevier Publishing Company LTD, Amsterdam-London-New York (1971).
4. M. A. Meyers, A. Mishra, and D. J. Benson, Prog. Mater. Sci. 51, 427 (2006).
5. J. Schiøtz, F. D. Di Tolla, and K. W. Jacobsen, Nature 391, 561 (1998).
6. L. Wang, Y. Gao, T. Xu, and Q. Xue, Mater. Chem. Phys.99, 96 (2006).
7. D. H. Jeong, F. Gonzalez, G. Palumbo, and K. T. Aust, U.Erb, Scr. Mater. 44, 493 (2001).
8. G. C. Hadjipanayis and R. W. Siegel, Nanophase Materials:Synthesis - Properties - Applications (NATO Science Series E:Applied Sciences, Vol. 260), p.233, Kluwer Academic, Dordrecht
(1994).
9. R. Mishra, B. Basu, and R. Balasubramaniam, Mater. Sci.Eng. A 373, 370 (2004).10. H. Conrad, J. Narayan, Scr. Mater. 42, 1025 (2000).
11. U. Erb, Nanostr. Mater. 6, 533 (1995).
12. D. L. Bish and J. E. Post, Modern Powder Diffraction, p.204, The Mineralogical Society of America, Washington, DC (1989).
13. A. W. Burton, K. Ong, T. Rea, and I. Y. Chan, Micropor. Mesopor. Mater. 177, 75 (2009).
14. Q. Luo and A. H. Jones, Surf. Coat. Technol. 205, 1403 (2010).
15. B. R. Jennings and K. Parslow, Proc. R. Soc. A 419, 137 (1988).
16. C. J. Bray and D. E. Karig, J. Geophys. Res. 90, 768 (1985).
17. H. S. Kim, Y. Estrin, and M. B. Bush, Acta Mater. 48, 493 (2000).
18. S. C. Wang, Z. Zhu, and M. J. Starink, Journal of Microsc. 217, 174 (2005).
19. P. G. Sanders, C. J. Youngdahl, and J. R. Weertman, Mater. Sci. Eng. A 234-236, 77 (1997).
20. A. Ibañez and E. Fatás, Surf. Coat. Technol. 191, 7 (2005).